Archives of Biochemistry and Biophysics 722 (2022) 109184

Contents lists available at ScienceDirect

Archives of Biochemistry and Biophysics

journal homepage: www.elsevier.com/locate/yabbi

Nucleosome destabilization by polyamines

Laszlo Imre [a,1], Erfaneh Firouzi Niaki [a,1], Rosevalentine Bosire [a], Peter Nanasi Jr. [a], Peter Nagy [a], Zsolt Bacso [a], Nubar Hamidova [a], Yves Pommier [b], Albert Jordan [c], Gabor Szabo [a,*]

[a] Department of Biophysics and Cell Biology, University of Debrecen, Faculty of Medicine Debrecen, H-4032, Hungary
[b] Center for Cancer Research, National Cancer Institute, National Institutes of Health, Bethesda, MD, 20892-4255, USA
[c] Molecular Biology Institute of Barcelona (IBMB-CSIC), Barcelona, 08028, Spain

ARTICLE INFO

Keywords:
Polyamine
Chromatin
Nucleosome
Stability
NCI-60
Histone

ABSTRACT

The roles and molecular interactions of polyamines (PAs) in the nucleus are not fully understood. Here their effect on nucleosome stability, a key regulatory factor in eukaryotic gene control, is reported, as measured in agarose embedded nuclei of H2B-GFP expressor HeLa cells. Nucleosome stability was assessed by quantitative microscopy [1,2] *in situ*, in close to native state of chromatin, preserving the nucleosome constrained topology of the genomic DNA. A robust destabilizing effect was observed in the millimolar concentration range in the case of spermine, spermidine as well as putrescine, which was strongly pH and salt concentration-dependent, and remained significant also at neutral pH. The integrity of genomic DNA was not affected by PA treatment, excluding DNA break-elicited topological relaxation as a factor in destabilization. The binding of PAs to DNA was demonstrated by the displacement of ethidium bromide, both from deproteinized nuclear halos and from plasmid DNA. The possibility that DNA methylation patterns may be influenced by PA levels is contemplated in the context of gene expression and DNA methylation correlations identified in the NCI-60 panel-based CellMiner database: methylated loci in subsets of high-ODC1 cell lines and the dependence of PER3 DNA methylation on PA metabolism.

1. Introduction

Polyamines (PAs) are indispensable metabolic products with multiple functions in the cell, from DNA synthesis to the regulation of transcription, translation, cell proliferation and differentiation, even including regulation of ion channels [3–6]. They receive much attention also in view of the therapeutic prospects of PA synthesis inhibition in cancer chemotherapy [7] and their relevance in the context of ageing [8]. The three main PAs, putrescine, spermidine, spermine, are generated from ornithine by ornithine decarboxylase 1 (ODC1), and from S-adenosylmethionine by its decarboxylase (Amd1/AdoMetDC). Their intracellular levels are elevated in various forms of cancer due to the overexpression of ODC1 which is under the control of the *MYC* gene [7,9,10]. Depletion of cellular polyamines causes growth arrest in mammalian cells [11].

There is an equilibrium between PAs that are bound to different polyanionic molecules and the free species; the pool of free PAs is thought to represent a minor fraction of the total cellular PA content which is regulated tightly and in an intricate manner, and set usually at sub-millimolar levels [12–14]. PAs are positively charged at physiological pH and associate with nucleotide triphosphates, acidic sites on proteins, phospholipid membranes and nucleic acids, mainly RNA [14,15]. PAs bind to the DNA parallel to its longitudinal axis [16], stabilizing the double helix and causing its bending [17], and also promoting its aggregation [18]. The binding of PAs, or their aggregates, to DNA may favor also the formation of noncanonical DNA structures [19]. PAs are thought to stabilize nucleosomes [20] and condense chromatin [21–25] in the ~0.1–3 mM PA concentration range, in spite of their physicochemical character what would enable competition with histones. The nucleosome destabilizing effect reported herein appears at slightly higher, but still biologically relevant PA concentrations in isolated nuclei depleted of linker histones, soluble enzymes and cofactors, in *in*

Abbreviations: PA, polyamine; ODC1, ornithine decarboxylase 1; Amd1, AdoMetDC S-adenosylmethionine decarboxylase; PTM, posttranslational modification; LSC, laser scanning cytometer/cytometry.

* Corresponding author. University of Debrecen, Faculty of Medicine, Department of Biophysics and Cell Biology, Life Science Building, room 2.309. 4032 Debrecen, Nagyerdei krt. 98, Hungary.
E-mail address: szabog@med.unideb.hu (G. Szabo).

[1] contributed equally.

https://doi.org/10.1016/j.abb.2022.109184
Received 29 December 2021; Received in revised form 8 March 2022; Accepted 11 March 2022
Available online 5 April 2022

situ conditions likely not favoring chromatin aggregation.

Stability features of nucleosomes are of regulatory importance and are assessed *in vitro* either by exposing reconstituted or isolated nucleosomes to challenging conditions and measuring their integrity, or studying their mobility features in live cells. The advantages of the fully native chromatin environment in the latter systems are overshadowed by various limitations including the complexity of factors influencing histone mobility and lack of robustness (see Ref. [1] for a detailed comparison of the different approaches). The quantitative microscopy-based assay we have developed (referred to as QINESIn) is suitable for a PTM-, histone variant- and cell cycle phase-specific analyses of nucleosome stability *in situ* [1] that yields reproducible and coherent picture of the measured feature in a variety of biological scenarios [1,2]; see also [26]. It is based on the exposure of agarose-embedded nuclei to salt (or, in another format of the assay, intercalator) solutions of increasing concentration and recording on a nucleus-by-nucleus basis of the amount of the tagged or native histone species remaining chromatin associated. In this work, we used H2B-GFP-expressor HeLa cells and salt elution to analyze the effect of PAs. In the experimental design, we took into consideration that PAs raise the pH of the buffer used even at low millimolar concentrations.

2. Materials and Methods

2.1. Embedding live cells into low melting point agarose

Prior to embedding, the wells of 8-well chambers (Ibidi, Martinsried, Germany) were coated with 1% (m/v) low melting point (LMP) agarose. 150 μl liquid agarose, diluted in distilled water was dispensed into each well and was immediately removed so that a thin agarose layer remained on the surfaces. The agarose layer was left to polymerize on ice for 2 min, then kept at 37 °C until the surface of the wells dried out. This coating procedure was repeated once more on the same chambers. Embedding was performed keeping cells and agarose at 37 °C. The cell suspension containing 6×10^6 cells/ml was mixed with 1% LMP agarose diluted in 1 × PBS (150 mM NaCl, 3.3 mM KCl, 8.6 mM Na_2HPO_4, and 1.69 mM KH_2PO_4, pH 7.4) at a v/v ratio of 1:3. 22 μl of the cell-agarose suspension was dispensed in the middle of the wells and the chambers were covered with homemade rectangular plastic coverslips cut out from a 200 μm thick, medium weight polyvinyl chloride binding cover (Fellowes, Inc., Itasca, Illinois, USA). The cells were left to sediment on the surface of the coated wells for 4 min at 37 °C, then kept on ice for 2 min. After polymerization of the agarose, 300 μl ice-cold complete culture medium was added to each well, a step aiding removal of the coverslips. For further details see Ref. [1].

2.2. Preparation of nuclei and histone eviction by salt

Following the protocol described in Ref. [1], the agarose-embedded cells at the bottom of the wells were washed with 500 μl ice-cold 1 × PBS, three times for 3 min, then treated with 500 μl ice-cold 1% (v/v) Triton X-100 dissolved in 1 × PBS/EDTA (5 mM EDTA in PBS, pH 7.4), for 10 min. This step was repeated once more, to produce permeabilized nuclei. Then the nuclei were washed with 500 μl ice-cold 1 × PBS/EDTA three times for 3 min and treated with different concentrations of NaCl solutions without or with polyamines, on ice, for 60 min, followed by three washes with 500 μl ice-cold 1 × PBS/EDTA. Since NaCl was diluted in 1 × PBS/EDTA, the salt concentrations indicated on the X-axes of the graphs in all the Figures show the total NaCl concentrations. Analysis of the curves was made by SigmaPlot 12.0, 'Standard curves: Four Parameter Logistic Curve' curve-fitting subroutines. Elution curves were normalized to '0′ subtracting the smallest value from all the others, and to '1′ dividing the mean fluorescence intensities represented by the data points by that of the non-treated sample. The numbers of analyzed G1 nuclei were between 200 and 1000/well, out of the ~500–2000 nuclei scanned. All the SEM values indicated in the Figure legends were calculated from the data points of the population of nuclei analyzed in the given experiment. EDTA was included in PBS to avoid nuclease induced nucleosome destabilization as well as nucleosome aggregation, both requiring divalent cations [1,27]. The elution experiments shown in Figs. 1 and 2 represent the results of one out of 3 or more independent experiments; the data in Fig. 3 were reproduced once.

2.3. Preparation of agarose plugs containing genomic DNA

Preparation of agarose-plugs was carried out by the standard method described in Ref. [28]. Cells were harvested and washed twice in PBS/EDTA. The cell samples were mixed with an equal volume of 1.5% low melting point (LMP) agarose (Sigma-Aldrich) dissolved in PBS/EDTA. Aliquots were allowed to harden in sample molds at 4 °C for 5 min. Each plug contained ~2.5×10^6 cells. To prepare nuclei, the cells were treated with 1% (v/v) Triton X-100 dissolved in PBS/EDTA for 60 min on ice. After extensive washing in PBS/EDTA (four times, 20 min on ice), the nuclei were treated with spermine dissolved in PBS/EDTA, for 60 min on ice using the concentrations indicated on the figure. After spermine treatment, the samples were extensively washed again in PBS/EDTA. The plugs were digested with 0.5 mg/ml Proteinase K (Thermo Fisher Scientific) in lysing solution (0.5 M EDTA, 10 mM Tris–HCl, 1% Sodium lauroyl sarcosinate, pH 8.0) at 55 °C for 2 days, then washed with TE (10 mM Tris–HCl, 2 mM EDTA, pH 8.0) and treated with 0.75 μM phenyl-methyl-sulfonyl-fluoride (PMSF, Sigma-Aldrich) at 37 °C for 10 min in order to inactivate residual proteinase activity. Finally, the plugs were washed with TE and stored in the same buffer at 4 °C.

2.4. Gel electrophoretic analysis

The agarose embedded samples were treated with S1 nuclease to convert nicks into double-strand breaks. Digestion was performed at a concentration of 1650 U S1/sample, for 1 h at 37 °C. For gel electrophoresis, a CHEF (contour clamped homogeneous electrical field)

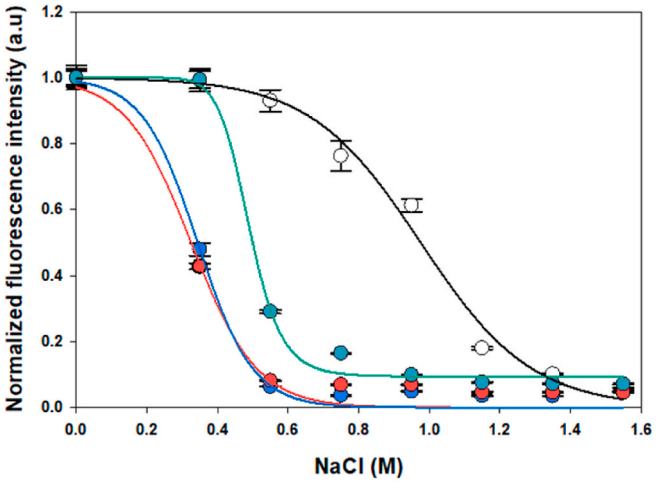

Fig. 1. The addition of PAs to agarose-embedded nuclei sensitizes nucleosomes to salt.
The stability of nucleosomes was analyzed in agarose-embedded nuclei of H2B-GFP expressor HeLa cells in the absence and presence of different PAs applied at a concentration of 10 mM. Spermine, spermidine and putrecsin are represented by green, blue and red lines, respectively; data obtained with PA-untreated, control samples are shown by the black line. The data points denote the means of green fluorescence intensities of ~1000 nuclei recorded by LSC. The G1 phase cells were gated for analyses according to the DNA distributions obtained by PI staining. The error bars are SEM values for 200–1000 G1 nuclei in one representative experiment.

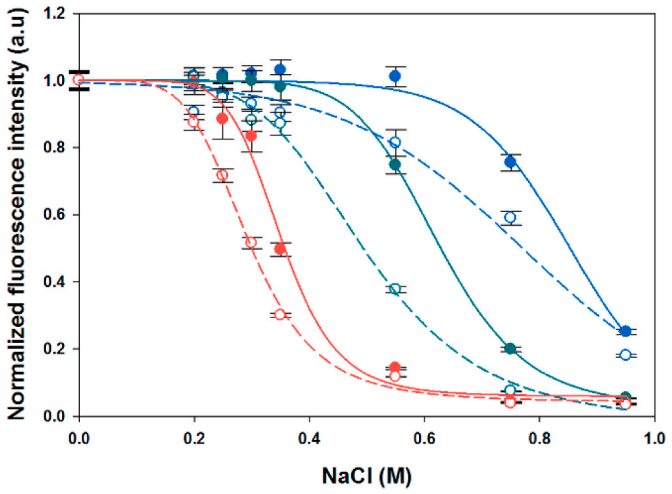

Fig. 2. Spermidine augments the eviction of histones induced by NaCl alone at the pH set by the PA.
Nuclei of H2B-GFP expressor HeLa cells suspended in PBS/EDTA were treated with a concentration series of NaCl alone with the pH of the buffer set to the value of the corresponding solution containing also spermidine (solid lines), or in combination with spermidine used at three different concentrations (dashed lines). The pH values of each solution are shown in Supplementary Fig. 1. The NaCl/PBS/EDTA solutions containing no spermidine were set to the pH of the corresponding 2.5, 5 and 10 mM spermidine containing solutions and are represented by blue, green and red lines, respectively. The samples containing also 2.5, 5 or 10 mM spermidine are represented by the same colours but with dashed lines. The PBS/EDTA + NaCl solutions were alkalized to the pH of the corresponding spermidine-containing solutions with NaOH. Means of the green fluorescence intensities of ~1000 nuclei recorded by LSC are plotted. The bars show SEM values.

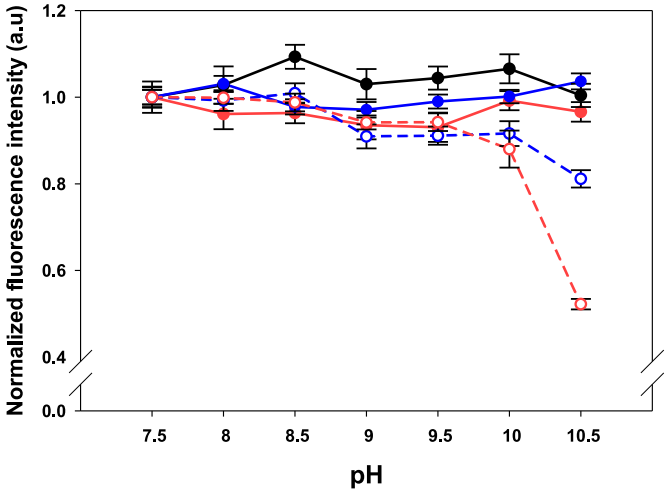

Fig. 3. Spermidine-induced histone eviction is pH-dependent.
Nuclei of H2B-GFP expressor HeLa cells were treated with 5 or 10 mM spermidine alone, in PBS/EDTA, without the addition of extra salt (filled blue and red symbols connected with solid lines, respectively) or with spermidine in combination with 550 mM (at 5 mM spermidine) or 350 mM (at 10 mM spermidine) NaCl (dashed lines, empty blue and red symbols, respectively). The black line and filled circles denote data obtained by treatment of nuclei with PBS-EDTA supplemented with 400 mM NaCl. The pH of the samples was adjusted to the values indicated on the X-axis. Means of the green fluorescence intensities of ~1500 nuclei were recorded by LSC and plotted as a function of the pH. The bars show SEM values.

mapper XA Pulse Field Electrophoresis System (Bio-Rad Laboratories Inc., Hercules, California, USA) was used (voltage gradient: 6 V/cm, run time: 24 h, initial switch time: 1s, final switch time: 25s, angle: 60°). As DNA size marker, the MidRange PFG Marker (New England Biolabs, UK) was used. The gel was stained with 5 μg/ml ethidium bromide (EBr).

2.5. Laser scanning cytometry (LSC)

LSC was performed using an iCys instrument (iCys® Research Imaging Cytometer; CompuCyte, Westwood, Massachusetts, USA). Green fluorescent protein (GFP) was excited using a 488 nm Argon ion laser. The fluorescence signals were collected via an UPlan FI 20 × (NA 0.5) objective. GFP was detected through a 510/21 nm filter. Each field comprising 1000 × 768 pixels was scanned with a step size of 1.5 μm. Data evaluation and hardware control were performed with the iCys 7.0 software for Windows XP. Gating of G1 phase cells was according to the fluorescence intensity distribution of the DNA labeled with propidium iodide (PI).

2.6. CellMiner analyses

CellMinerCDB analyses were performed using the publicly accessible web portal https://discover.nci.nih.gov/rsconnect/cellminercdb/ (see Ref. [29] and refs. cited therein). The gene expression data were exported to Excel for comparison of the average toxicity features of the 10 vs. 50 cell lines exhibiting striking difference in HIST1H1B mRNA levels, and the drugs differentiating best between the two categories of cells based on the calculated means and variances were further analyzed experimentally as described in Results and Discussion. These drugs (Gallamine, Hinokitiol) were obtained through the courtesy of the NIH Developmental Therapeutics Program, while ß-Lapachone was purchased from Sigma-Aldrich.

3. Results and Discussion

The effect of PAs on the stability of nucleosomes was analyzed by the salt elution assay named QINESIn [1,2], in permeabilized nuclei of H2B-GFP expressing HeLa cells. As Fig. 1 shows, the addition of PAs to the agarose-embedded nuclei at a concentration of 10 mM markedly lowered the concentration of salt required to destabilize the nucleosomes as reflected by the release of H2B-GFP, putrescine being the least active. However, the pH of the PBS/EDTA buffer was strongly increased by the addition of PAs; so destabilization could be partly attributed to the shift of pH toward the isoelectric point of the histones (~10 for H2B, ~10.5 for H2A and ~11 for H3 and H4; see Refs. [30,31]). Therefore, to determine whether PAs themselves exert a destabilizing effect, the salt elution curves were compared in the presence and the absence of the PA at matched pH values documented in Supplementary Fig. 1.

The data shown in Fig. 2 demonstrate that spermidine, at a concentration as low as 2.5 mM, augments NaCl-induced H2B-GFP release, indicating that nucleosome destabilization cannot be due merely to alkaline pH but also to spermidine itself. There was no nucleosome release below 400 mM salt and pH = 9.3 in the absence of PA, but there was a significant destabilization at this pH and salt concentration by 5 mM spermidine.

Fig. 3 shows that alkalization alone, even in the presence of 400 mM salt, does not cause H2B-GFP release up to pH = 10.5. Spermidine used at a concentration of 5 and 10 mM, in combination with 400 and 200 mM salt, respectively, destabilizes the nucleosomes robustly above pH = 10. It took 10 mM spermidine and pH > 10.5 to destabilize the nucleosomes in PBS/EDTA without the addition of extra NaCl (not shown). The slight increment in the amount of H2B-GFP remaining in the nuclei treated either with salt or spermidine alone may be the result of complex effects involving chromatin aggregation and nucleosome destabilization at the same time.

Topological relaxation of the DNA, by e.g. introducing single-strand

(ss) or double-strand (ds) breaks, strongly destabilizes nucleosomes [1,32,33]. Therefore, in view of published data suggesting that PAs may affect DNA integrity [34], the ds size of the genomic DNA isolated from PA-treated nuclei was analyzed by CHEF [35] using S1 nuclease digestion to generate double-strand breaks at all the ss regions present in the genome [36]. As Supplementary Fig. 2 shows, neither ss nor ds breaks were generated as a result of the treatment, even at the pH set by the PA used.

Nucleosomal DNA interacts with the histone octamer at 14 distinct sites via electrostatic and hydrogen bonds mainly involving histone residues and the phosphodiester backbone where the minor groove faces the octamer [37,38], and via salt-bridge interactions with the N-terminal histone tails [39,40]. The nucleosome particle keeps the DNA wound around it in a constrained negative toroid supercoil [41]. As anticipated based on these molecular interactions, nucleosomes readily disassemble upon exposure to salt or intercalators [42], which is exploited in the assay used herein for the quantitative assessment of nucleosome stability *in situ* [1]. Within the physiological range up to pH = 8.0, nucleosomes are expected to be stable [43]. Alkalization to near the isoelectric point of the histones sensitized the nucleosomes to salt-induced disruption, as Figs. 2 and 3 show, decreasing the electrostatic binding forces. Alkaline conditions alone at physiological ionic strength did not dissociate H2B-GFP from the nucleosomes (Fig. 3), both alkaline pH and elevated salt concentration were necessary for nucleosome disassembly. Such a combined effect was also observed in the case of destabilization induced by DNA intercalators, requiring ≥800 mM NaCl [1].

Since PAs interact with DNA changing its superhelical twist [44–46], we hypothesized that their nucleosome destabilizing effect may be explained by topological distortion. PA DNA binding was demonstrated by measuring ethidium bromide (EBr) displacement, a widely used indicator of ligand-DNA interaction [47], performed in a sensitive nuclear halo format; see Supplementary Fig. 3. As Supplementary Fig. 4 shows, the efficiency of EBr displacement was similar in the case of supercoiled or relaxed DNA, suggesting that PAs may not have a strong bias to a particular topological form. The pH of PA solutions was neutral in these experiments; PAs are known to bind and condense linear DNA at neutral pH [48]. Thus, topological changes imposed on the DNA by PAs cannot possibly explain the nucleosome destabilizing effect observed. We assume that direct competition with histones is responsible for their augmented disassembly. Reminiscent of our observations, fluorescence resonance energy transfer measurements on histone H1 depleted chromatosomes detected a more open nucleosome conformation due to detachment of the two terminal arms of DNA from the histone octamers in the presence of polyamines [49].

Altered nucleosome stability may affect the establishment and regulatory modulation of the epigenetic landscape by altered access of enzymes involved in DNA methylation and demethylation, to their target motives [50,51]. This assumption follows from the fact that nucleosomes are strong barriers to DNA methyltransferases, and recent cryo-EM studies revealed steric constraints imposed by the nucleosomal structure which explain the requirement for remodeling of nucleosomes for *de novo* methylation to occur [52]. Contemplating this scenario, we asked whether (a) dependence of DNA methylation on PA metabolism can be detected, and (b) aberrant DNA methylation may appear in concert with high ODC1 expression. To address the questions systematically, we looked for correlations between the levels of the two rate-limiting enzymes involved in PA synthesis, ODC1 or AMD1 [14] and methylation of CpG islands, within the NCI-60 panel of cell lines using the CellMiner database [53,54]. Regarding (a), using the lasso algorithm of multivariate analyses at https://discover.nci.nih.gov/rsconnect/cellminercdb/, we identified *PER3* among the ODC1 correlates and observed a significant correlation between ODC1 and PER3 mRNA expression levels in the univariate mode ($R = 0.55$; $p = 6.3 \times 10^{-6}$; Supplementary Fig. 5A), and also between *ODC1* expression and *PER3* DNA methylation ($R = 0.59$; $p = 6.5 \times 10^{-7}$; Supplementary Fig. 5B). These observations are in line with the concept that these processes are interlinked [55–60], and can be considered as a manifestation of the pervasive dynamics of CpG methylation [61]. PA levels oscillate in a daily manner, a feature declining with age [62], and changes in PER3 DNA methylation has been observed in certain physiological and pathological conditions [63–65]. The possibility that the above correlation may be related to changes of nucleosome stability is in line with the findings on the circadian clock-dependence of ATACseq-assessed chromatin accessibility landscapes [66]. We propose that nucleosome destabilization is to be included among the several mechanisms thought to contribute to PAs dramatic effects on circadian regulatory genes [60]. Regarding (b), although there is no correlation ($R \approx 0.25$) between CpG island methylation over a large DNA region encompassing all the histone genes vs. ODC1 or AMD1 expression across the 60 cell lines, a distinct group of ten cell lines exhibit strikingly low (or no) expression of certain histones and histone variants as well as some other genes at the mRNA level, and this feature appears to correlate with high ODC1 expression (See Supplementary Fig. 6 for the relationship between HIST1H1B and ODC1 expression.). The low expression of the silenced genes is obviously due to DNA methylation, as shown for H1.5 in Supplementary Fig. 7. Remarkably, the phenomenon does not depend on the cell lineage. Thus it appears that metabolic conditions favoring high PA flux promote DNA methylation leading to gene silencing.

Besides silencing HIST1H1B coding for the linker histone variant H1.5, DNA methylation suppresses the neighboring histone genes, HIST1H4L, HIST1H3i. Genes coding for histone isoforms, including HIST1H4L, were found to be hypermethylated in various malignancies like hepatocellular carcinoma and triple-negative breast cancer cells [67]. Methylated patches, silencing the corresponding genes, can be discovered also in other loci (NDN, TOX3, PGR, SMC1B, TYR, RPL26P19, RPL26P4, and RPS2P34) in the group of the very same ten cell lines. Remarkably, the methylated CpG-binding protein MBD2 is highly expressed in the same cell lines (Supplementary Fig. 8). Notably, MBD2 is a key player in the maintenance and spread of DNA methylation at CpG islands in cancer [68].

Other examples of the peculiar dichotomy in gene expression and DNA methylation among the high *ODC1* expressor cell lines were also identified. For example at an imprinted chromatin domain, 14 cell lines among the high ODC1-expressors show silenced SNURF and SNRPN genes due to DNA methylation; these lines only partially overlap with the ten lines showing low HIST1H1B, HIST1H4L, HIST1H3i levels (based on CellMinerCDB analyses). Furthermore, the 14 cell lines express MBD5 (rather than MBD2) at higher levels relative to the average of the other 36 cell lines. Since expression of ODC1 and of AMD1 correlate across the panel ($r = 0.61$ when the skin-derived outlier lines are excluded from the calculation), it is likely that the high expressor cells have higher intracellular PA levels in comparison with the other fifty cell lines. We speculate that elevated PA levels might contribute to the special DNA methylation pattern of the ODC1-high cell lines what may be partly explained by their nucleosome destabilizing effect based on the data presented herein. However, the metabolic and regulatory scenario is highly complex and ranking of the various possible relationships regarding their contribution to the common epigenetic features of a subpopulation of cell lines is difficult. For example, there are metabolic avenues predicting CpG demethylation at high PA levels [69,70], while inhibition of polyamine synthesis by ornithine decarboxylase antizyme-1 e.g., results in hypomethylation of genomic DNA [71]. Furthermore, the different layers of epigenetic regulations, like histone acetylation, DNA methylation, and even topoisomerase I activity, are interconnected [72–75]; therefore the nucleosome destabilizing influence of elevated PA levels is but one among the several possible effects, albeit the most direct. In summary, the peculiar pattern of DNA methylation in a subgroup of high-ODC1 cancer cell lines may indicate that high PA levels may facilitate the establishment of such patterns, with gene silencing consequences of biological significance.

In view of the above complexities, we asked if the relationships between the high ODC1 levels and the peculiar CpG pattern in the ten cell

lines could be better understood on the grounds of possible common phenotypic features. Indeed, the ten cell lines distinguished by the aberrant methylation patterns involving certain genes are hypersensitive to particular drugs (e.g. Gallamine, Hinokitiol and ß-Lapachone) based on our analyses of the CellMiner dataset (see Materials and Methods). This special sensitivity may be the result of a common, aberrant methylation pattern established in these cells by their high MBD2 expression (see Supplementary Fig. 8); alternatively, these features that are common for the ten cell lines can also be interpreted in terms of the suppression of select linker histone variants disturbing chromatin structure and its regulation in a distinct fashion. In line with the latter possibility, a marked effect of H1.5 on overall chromatin architecture was observed [76]. Of note, histone variants were implicated in epigenetic diversification related to carcinogenesis [77–79], and the alterations of their expression could be linked to DNA methylation [80,81]. However, this possibility was not corroborated in our efforts to detect differences between cells induced to express different levels of H1.5 (using the experimental system of [82]) in their sensitivity to these drugs (data not shown). Therefore, the identified common phenotypic features (sensitivity to the same set of drugs) may involve silenced genes other than HIST1H1B. In accordance with this possibility, toxicity of Hinokitiol, one of the above compounds, an iron chelator and transporter [83,84], strongly correlates with PER3 DNA methylation (Supplementary Fig. 9). Thus, a phenotypic feature characteristic for the ten cell lines distinguished from the rest of the NCI-60 panel based on DNA methylation patterns correlates also with PER3 methylation which is also dependent on PA metabolism.

The nucleosomal structure being repressive for transcriptional activities, its stability is of central regulatory significance impacting also the enzymatic activities involved in the ATP dependent process of chromatin remodeling [51,85,86]. Thus, the destabilizing effect of PAs demonstrated herein may affect the fine balance of factors regulating remodeling [87], making grounds for subsequent enzymatic activities. The histone acetylase stimulating activity of PAs, e.g. may be indirect [88]. In connection with such a scenario, there is significant correlation between expression of SMARCC1, a remodeler overexpressed in prostate cancer [89,90], and the activity of Hinokitiol ($R = 0.58$; $p = 4.5 \times 10^{-5}$). SMARCC1 expression also correlates with PER3 DNA methylation ($R = 0.41$; $p = 0.0012$) which also correlates with Hinokitiol toxicity (Supplementary Fig. 9). Thus, one of the drugs exhibiting increased toxicity to the ten cell lines characterized both with aberrant methylation patterns and high ODC1 expression is generally more toxic for cells expressing the SMARCC1 remodeler, raising the possibility that high PA levels might affect DNA-dependent enzymatic processes via alterations induced in chromatin remodeling. Such a mechanism could lead to changes in DNA methylation since nucleosomes are strong barriers to DNA methyltransferases in the absence of remodeling, what explains the spatiotemporal connection between DNA methylation and remodeling [50]. The nucleosome destabilizing effect of PAs could help establish a chromatin structure that is optimal for the enzymes. *De novo* methylation preferentially involves the internucleosomal linker regions and this is antagonized by histone H1 [91]; thus, aberrant methylation of the promoters of H1 variant genes could lead to further methylations at regions not blocked by the linker histones any more.

The millimolar concentration range of the nucleosome destabilizing effect observed in our experiments is attained by PAs in various physiological and pathological scenarios [92–95]. PAs can reach 10–12 mM concentration in cultured Jurkat and human mammary epithelial cells [70] and in prostate cancer due to the extraordinary biosynthetic flux involving polyamine metabolism [96,97]. Pertinently to the hypothesis tackled, aberrant DNA methylation has been recognized as a prominent factor in prostate cancer development [71,98]. PAs appear to preferentially accumulate in the nucleoli taking part in the regulation of rRNA synthesis [99,100], reaching high local concentrations, and are considered there as the nexus to certain autoimmune diseases [101]. PAs are present in a millimolar concentration in plants, fulfilling diverse functions which can be modulated by their exogenous application in high concentrations [69,102,103]. Thus, the PA concentration sufficient to elicit nucleosome destabilization is reached in multiple physiological and pathological scenarios.

We speculate that overproduction of PAs primes aberrant DNA methylation patterns, leading to epigenetic diversification in the clonal evolution of cancer via an ODC1-DNA methylation axis. The loci preferentially methylated might not be randomly selected in view of the recurrent genes silenced in the groups of the ten vs. fourteen cell lines of different lineages exhibiting differential MBD2 or MBD5 expression (see above). Our hypothesis that high PA levels might induce epigenetic diversification is in line with observations of intratumor clonal heterogeneities in cancer tissues, e.g. in prostate carcinoma, since these heterogeneities are attributed to differential DNA methylation [77,98]. The role of polyamines in differential DNA methylation during normal cell differentiation has also been noted [104].

Chromatin compaction in permeabilized nuclei treated with polyamines ensues at 0.2 and 0.5 mM spermine or spermidine concentrations, and appears not to change further above 0.8 and 1.5 mM concentration, respectively [21]. Thus, the nucleosome destabilizing effect of PAs, becoming prominent at $\geq$ 5 mM concentration, can be clearly distinguished from how they contribute to higher-order chromatin architecture. The nucleosome destabilizing effect described herein is apparently superimposed on PAs' contribution to the condensed state of chromatin as well as on other, indirect PA effects on chromatin structure and function; these include the upregulation of histone acetylation [72] and complex effects on DNMTs [69,70,105] ensuing at ODC1 overexpression, or PA feeding, respectively. Our experimental system of isolated nuclei, devoid of H1, soluble enzymes and cofactors, allowed us to assess nucleosome stability in the absence of most of the biochemical processes contributing to the changes of chromatin structure evoked by PA treatment (reviewed in Ref. [106]). The nucleosome destabilizing effect of PAs described herein may contribute to the circadian regulation of transcriptional processes exemplified by that of the *PER3* gene with its strongly ODC1-dependent methylation revealed in our CellMiner analyses. The experimental demonstration of a nucleosome destabilizing effect exerted by high but still physiological levels of PAs is proposed to fit a scenario where high ODC1 expression facilitates chromatin remodeling, allowing access of methylating enzymes to the DNA at sites associated with physiological processes like circadian rhythm or at aberrantly selected loci in the context of cancer cell evolution.

Declaration of competing interest

The authors declare no competing interests.

Acknowledgment

Technical assistance by Ms. Adel Vezendine is warmly acknowledged. This work was supported by OTKA K 128770, K 138524, COST CA 15214, Stipendium Hungaricum scholarship by the Tempus Public Foundation (to RB) and the Richter Talentum Fund (EFN and NH). We are thankful to the NIH Developmental Therapeutics Program for providing the drugs investigated.

Appendix A. Supplementary data

Supplementary data to this article can be found online at https://doi.org/10.1016/j.abb.2022.109184.

References

[1] L. Imre, Z. Simandi, A. Horvath, G. Fenyofalvi, P. Nanasi, E.F. Niaki, et al., in: Nucleosome Stability Measured in Situ by Automated Quantitative Imaging vol. 7, Oct 6 2017, 12734.

[2] L. Henn, A. Szabó, L. Imre, Á. Román, A. Ábrahám, B. Vedelek, et al., Alternative linker histone permits fast paced nuclear divisions in early Drosophila embryo, Nucleic Acids Res. 48 (Sep 18 2020) 9007–9018.

[3] R.A. Casero Jr., T. Murray Stewart, A.E. Pegg, Polyamine metabolism and cancer: treatments, challenges and opportunities, Nat. Rev. Cancer 18 (Nov 2018) 681–695.

[4] N.K. Lee, H.E. MacLean, Polyamines, androgens, and skeletal muscle hypertrophy, J. Cell. Physiol. 226 (Jun 2011) 1453–1460.

[5] K. Igarashi, K. Kashiwagi, The functional role of polyamines in eukaryotic cells, Int. J. Biochem. Cell Biol. 107 (Feb 2019) 104–115.

[6] A.E. Pegg, Functions of polyamines in mammals, J. Biol. Chem. 291 (Jul 15 2016) 14904–14912.

[7] E. Damiani, H.M. Wallace, Polyamines and cancer, Methods Mol. Biol. 1694 (2018) 469–488.

[8] N. Minois, D. Carmona-Gutierrez, F. Madeo, Polyamines in aging and disease, Aging (Albany NY) 3 (Aug 2011) 716–732.

[9] A.S. Bachmann, D. Geerts, in: Polyamine Synthesis as a Target of MYC Oncogenes vol. 293, Nov 30 2018, pp. 18757–18769.

[10] F. Sánchez-Jiménez, M. Medina, Polyamines in Mammalian Pathophysiology, vol. 76, Oct 2019, pp. 3987–4008.

[11] S. Mandal, A. Mandal, H.E. Johansson, A.V. Orjalo, M.H. Park, Depletion of cellular polyamines, spermidine and spermine, causes a total arrest in translation and growth in mammalian cells, Proc. Natl. Acad. Sci. Unit. States Am. 110 (2013) 2169.

[12] C. Kahana, Protein degradation, the main hub in the regulation of cellular polyamines, Biochem. J. 473 (Dec 15 2016) 4551–4558.

[13] C. Kahana, The antizyme family for regulating polyamines, J. Biol. Chem. 293 (Nov 30 2018) 18730–18735.

[14] A.E. Pegg, Mammalian polyamine metabolism and function, IUBMB Life 61 (2009) 880–894.

[15] S. Watanabe, K. Kusama-Eguchi, H. Kobayashi, K. Igarashi, Estimation of polyamine binding to macromolecules and ATP in bovine lymphocytes and rat liver, J. Biol. Chem. 266 (Nov 5 1991) 20803–20809.

[16] T. Nishio, Y. Yoshikawa, C.Y. Shew, N. Umezawa, T. Higuchi, K. Yoshikawa, Specific effects of antitumor active norspermidine on the structure and function of DNA, Sci. Rep. 9 (Oct 18 2019), 14971.

[17] V. Vijayanathan, T.J. Thomas, S.K. Nair, A. Shirahata, M.A. Gallo, T. Thomas, Bending of the estrogen response element by polyamines and estrogen receptors alpha and beta: a fluorescence resonance energy transfer study, Int. J. Biochem. Cell Biol. 38 (2006) 1191–1206.

[18] J. Pelta, F. Livolant, J.L. Sikorav, DNA aggregation induced by polyamines and cobalthexamine, J. Biol. Chem. 271 (Mar 8 1996) 5656–5662.

[19] W. Brooks, Increased polyamines alter chromatin and stabilize autoantigens in autoimmune diseases, Front. Immunol. 4 (2013-April-17 2013).

[20] X. Ni, R.D. Cole, Effects of various salts and pH on the stability of the nucleosome in chromatin fragments, Biochemistry 33 (1994/08/01 1994) 9276–9284.

[21] A. Visvanathan, K. Ahmed, L. Even-Faitelson, D. Lleres, D.P. Bazett-Jones, A. I. Lamond, Modulation of higher order chromatin conformation in mammalian cell nuclei can Be mediated by polyamines and divalent cations, PLoS One 8 (2013), e67689.

[22] D.M. Sauvé, H.J. Anderson, J.M. Ray, W.M. James, M. Roberge, Phosphorylation-induced rearrangement of the histone H3 NH2-terminal domain during mitotic chromosome condensation, J. Cell Biol. 145 (Apr 19 1999) 225–235.

[23] E. Raspaud, I. Chaperon, A. Leforestier, F. Livolant, Spermine-induced aggregation of DNA, nucleosome, and chromatin, Biophys. J. 77 (1999/09/01/ 1999) 1547–1555.

[24] A. Leforestier, S. Fudaley, F. Livolant, Spermidine-induced aggregation of nucleosome core particles: evidence for multiple liquid crystalline phases, J. Mol. Biol. 290 (Jul 9 1999) 481–494.

[25] W. Pan, J. Zhou, Y. Yin, H. Wen, D. Liang, Local de-condensation of double-stranded DNA in oppositely charged polyelectrolyte as induced by spermidine, Soft Matter 11 (Jun 21 2015) 4705–4709.

[26] D. Sharma, L. De Falco, S. Padavattan, C. Rao, S. Geifman-Shochat, C.F. Liu, et al., PARP1 exhibits enhanced association and catalytic efficiency with gammaH2A.X-nucleosome, Nat. Commun. 10 (Dec 17 2019) 5751.

[27] T. Ohyama, New aspects of magnesium function: a key regulator in nucleosome self-assembly, chromatin folding and phase separation, Int. J. Mol. Sci. 20 (Aug 29 2019).

[28] T. Mamiatis, E.F. Fritsch, J. Sambrook, J. Engel, Molecular Cloning–A Laboratory Manual, S., 42, in: Acta Biotechnologica, vol. 545. vol. 5, Cold Spring Harbor Laboratory, New York, 1982, 104-104, 1985/01/01 1985.

[29] A. Luna, F. Elloumi, S. Varma, Y. Wang, V.N. Rajapakse, M.I. Aladjem, et al., CellMiner Cross-Database (CellMinerCDB) version 1.2: exploration of patient-derived cancer cell line pharmacogenomics, Nucleic Acids Res. 49 (Jan 8 2021) D1083–D1093.

[30] H. Nishida, Relationship between chromosomal GC content and isoelectric points of histones in fungi, J. Gen. Appl. Microbiol. 61 (2015) 24–26.

[31] S.Y. Chung, W.E. Hill, P. Doty, Characterization of the histone core complex, Proc. Natl. Acad. Sci. U. S. A. 75 (Apr 1978) 1680–1684.

[32] É. Hegedüs, E. Kókai, P. Nánási, L. Imre, L. Halász, R. Jossé, et al., Endogenous single-strand DNA breaks at RNA polymerase II promoters in Saccharomyces cerevisiae, Nucleic Acids Res. 46 (Nov 16 2018) 10649–10668.

[33] R. Bosire, P. Nánási Jr., L. Imre, B. Dienes, Á. Szöőr, A. Mázló, et al., Intercalation of Small Molecules into DNA in Chromatin Is Primarily Controlled by Superhelical Constraint vol. 14, 2019, e0224936.

[34] R. Male, V.M. Fosse, K. Kleppe, Polyamine-induced hydrolysis of apurinic sites in DNA and nucleosomes, Nucleic Acids Res. 10 (Oct 25 1982) 6305–6318.

[35] D. Blöcher, M. Einspenner, J. Zajackowski, CHEF electrophoresis, a sensitive technique for the determination of DNA double-strand breaks, Int. J. Radiat. Biol. 56 (Oct 1989) 437–448.

[36] E. Hegedüs, L. Imre, J. Pataki, E. Lizanecz, L. Székvölgyi, F. Fazakas, et al., Heteroduplex analysis using flow cytometric microbead assays to detect deletions, insertions, and single-strand lesions, Cytometry 73 (Mar 2008) 238–245.

[37] K. Luger, A.W. Mäder, R.K. Richmond, D.F. Sargent, T.J. Richmond, Crystal structure of the nucleosome core particle at 2.8 Å resolution, Nature 389 (1997/09/01 1997) 251–260.

[38] C.A. Davey, D.F. Sargent, K. Luger, A.W. Maeder, T.J. Richmond, Solvent mediated interactions in the structure of the nucleosome core particle at 1.9 a resolution, J. Mol. Biol. 319 (Jun 21 2002) 1097–1113.

[39] B.J. Placek, L.M. Gloss, The N-terminal tails of the H2A-H2B histones affect dimer structure and stability, Biochemistry 41 (Dec 17 2002) 14960–14968.

[40] S. Sharma, F. Ding, N.V. Dokholyan, Multiscale modeling of nucleosome dynamics, Biophys. J. 92 (Mar 1 2007) 1457–1470.

[41] G. Muskhelishvili, A. Travers, in: The Regulatory Role of DNA Supercoiling in Nucleoprotein Complex Assembly and Genetic Activity vol. 8, Nov 2016, pp. 5–22.

[42] T. Elbel, J. Langowski, The effect of DNA supercoiling on nucleosome structure and stability, J. Phys. Condens. Matter 27 (Feb 18 2015), 64105.

[43] X. Ni, R.D. Cole, Effects of various salts and pH on the stability of the nucleosome in chromatin fragments, Biochemistry 33 (Aug 9 1994) 9276–9284.

[44] Q. Shao, S. Goyal, L. Finzi, D. Dunlap, Physiological levels of salt and polyamines favor Writhe and limit twist in DNA, Macromolecules 45 (2012/04/10 2012) 3188–3196.

[45] E. Clark, R.A. Swank, J.E. Morgan, H. Basu, H.R. Matthews, Two new photoaffinity polyamines appear to alter the helical twist of DNA in nucleosome core particles, Biochemistry 30 (Apr 23 1991) 4009–4020.

[46] H.R. Matthews, Polyamines, chromatin structure and transcription, Bioessays 15 (Aug 1993) 561–566.

[47] P. Allegra, E. Amodeo, S. Colombatto, S.P. Solinas, The ability of cystamine to bind DNA, Amino Acids 22 (2002) 155–166.

[48] Z. Guo, Y. Wang, A. Yang, G. Yang, The effect of pH on charge inversion and condensation of DNA, Soft Matter 12 (Aug 21 2016) 6669–6674.

[49] H. Zhang, T. Li, Effects of spermidine and ATP on stabilities of chromatosomes and histone H1-depleted chromatosomes, Bioorg. Med. Chem. Lett 27 (Mar 1 2017) 1149–1153.

[50] D.B. Lyons, D. Zilberman, DDM1 and Lsh Remodelers Allow Methylation of DNA Wrapped in Nucleosomes vol. 6, Nov 15 2017.

[51] A. Schrader, T. Gross, V. Thalhammer, G. Längst, Characterization of Dnmt1 binding and DNA methylation on nucleosomes and nucleosomal arrays, PLoS One 10 (2015), e0140076.

[52] T.H. Xu, M. Liu, X.E. Zhou, G. Liang, Structure of Nucleosome-Bound DNA Methyltransferases DNMT3A and DNMT3B vol. 586, Oct 2020, pp. 151–155.

[53] V.N. Rajapakse, A. Luna, M. Yamade, L. Loman, S. Varma, M. Sunshine, et al., CellMinerCDB for integrative cross-database genomics and pharmacogenomics analyses of cancer cell lines, iScience 10 (Dec 21 2018) 247–264.

[54] A. Luna, F. Elloumi, S. Varma, Y. Wang, Vinodh N. Rajapakse, M.I. Aladjem, et al., CellMiner Cross-Database (CellMinerCDB) Version 1.2: Exploration of Patient-Derived Cancer Cell Line Pharmacogenomics, Nucleic Acids Research, 2020.

[55] H. Peng, Y. Zhu, J. Goldberg, V. Vaccarino, J. Zhao, DNA methylation of five core circadian genes jointly contributes to glucose metabolism: a gene-set analysis in monozygotic twins, Front. Genet. 10 (2019) 329.

[56] F. Rijo-Ferreira, J.S. Takahashi, Genomics of circadian rhythms in health and disease, Genome Med. 11 (Dec 17 2019) 82.

[57] A. Mashhour, Z. Al Mansour, A.S. Al Hallaj, R. Ali, T. Trivilegio, M. Boudjelal, P19 cells as a model for studying the circadian clock in stem cells before and after cell differentiation, J. Circadian Rhythms 16 (6) (May 18 2018).

[58] S.T. Chen, K.B. Choo, M.F. Hou, K.T. Yeh, S.J. Kuo, J.G. Chang, Deregulated expression of the PER1, PER2 and PER3 genes in breast cancers, Carcinogenesis 26 (Jul 2005) 1241–1246.

[59] Y. Li, Y. Shan, G.K. Kilaru, S. Berto, G.Z. Wang, K.H. Cox, et al., Epigenetic inheritance of circadian period in clonal cells, Elife 9 (May 27 2020).

[60] L. Galluzzi, F. Pietrocola, G. Kroemer, Molecular regulation of circadian rhythms by polyamines, Cell Metabol. 22 (Nov 3 2015) 757–758.

[61] C. Luo, P. Hajkova, J.R. Ecker, Dynamic DNA methylation: in the right place at the right time, Science 361 (Sep 28 2018) 1336–1340.

[62] Z. Zwighaft, R. Aviram, M. Shalev, L. Rousso-Noori, J. Kraut-Cohen, M. Golik, et al., Circadian clock control by polyamine levels through a mechanism that declines with age, Cell Metabol. 22 (Nov 3 2015) 874–885.

[63] O. Ramos-Lopez, M. Samblas, F.I. Milagro, J.I. Riezu-Boj, A.B. Crujeiras, J. A. Martinez, et al., Circadian gene methylation profiles are associated with obesity, metabolic disturbances and carbohydrate intake, Chronobiol. Int. 35 (Jul 2018) 969–981.

[64] D. Shi, J. Chen, J. Wang, J. Yao, Y. Huang, G. Zhang, et al., Circadian clock genes in the metabolism of non-alcoholic fatty liver disease, Front. Physiol. 10 (2019) 423.
[65] C.A. Koczor, I. Ludlow, R.S. Hight 2nd, Z. Jiao, E. Fields, T. Ludaway, et al., Ecstasy (MDMA) alters cardiac gene expression and DNA methylation: implications for circadian rhythm dysfunction in the heart, Toxicol. Sci. 148 (Nov 2015) 183–191.
[66] E.N. Weizman, M. Tannenbaum, A.M. Tarrant, O. Hakim, O. Levy, Chromatin dynamics enable transcriptional rhythms in the cnidarian Nematostella vectensis, PLoS Genet. 15 (Nov 2019), e1008397.
[67] R. Singh, E. Bassett, A. Chakravarti, M.R. Parthun, Replication-dependent histone isoforms: a new source of complexity in chromatin structure and function, Nucleic Acids Res. 46 (2018) 8665–8678.
[68] C. Stirzaker, J.Z. Song, W. Ng, Q. Du, N.J. Armstrong, Methyl-CpG-binding Protein MBD2 Plays a Key Role in Maintenance and Spread of DNA Methylation at CpG Islands and Shores in Cancer vol. 36, Mar 2017, pp. 1328–1338.
[69] K. Soda, Polyamine metabolism and gene methylation in conjunction with one-carbon metabolism, Int. J. Mol. Sci. 19 (Oct 10 2018).
[70] T. Fukui, K. Soda, in: Extracellular Spermine Activates DNA Methyltransferase 3A and 3B vol. 20, Mar 12 2019.
[71] D. Yamamoto, K. Shima, K. Matsuo, T. Nishioka, C.Y. Chen, G.F. Hu, et al., Ornithine decarboxylase antizyme induces hypomethylation of genome DNA and histone H3 lysine 9 dimethylation (H3K9me2) in human oral cancer cell line, PLoS One 5 (Sep 3 2010), e12554.
[72] C.A. Hobbs, S.K. Gilmour, High levels of intracellular polyamines promote histone acetyltransferase activity resulting in chromatin hyperacetylation, J. Cell. Biochem. 77 (Apr 2000) 345–360.
[73] K. Tamari, M. Konno, A. Asai, J. Koseki, K. Hayashi, K. Kawamoto, et al., Polyamine flux suppresses histone lysine demethylases and enhances ID1 expression in cancer stem cells, Cell Death Discov. 4 (104) (2018/11/13 2018).
[74] Y. Huang, E. Greene, T. Murray Stewart, A.C. Goodwin, S.B. Baylin, P.M. Woster, et al., Inhibition of lysine-specific demethylase 1 by polyamine analogues results in reexpression of aberrantly silenced genes, Proc. Natl. Acad. Sci. Unit. States Am. 104 (2007) 8023.
[75] D.G. Kim, J. Du, C. Miao, J.H. Jung, S.C. Park, D.K. Kim, The possible roles for polyamines in the initiation process of SV40 DNA replication in vitro, Oncol. Rep. 19 (Feb 2008) 535–539.
[76] J.Y. Li, M. Patterson, H.K. Mikkola, W.E. Lowry, S.K. Kurdistani, Dynamic distribution of linker histone H1.5 in cellular differentiation, PLoS Genet. 8 (2012), e1002879.
[77] C.M. Torres, A. Biran, M.J. Burney, H. Patel, T. Henser-Brownhill, A.S. Cohen, et al., The linker histone H1.0 generates epigenetic and functional intratumor heterogeneity, Science 353 (Sep 30 2016).
[78] P. Scaffidi, Histone H1 alterations in cancer, Biochim. Biophys. Acta (BBA) - Gene Regulat. Mechan. 1859 (2016/03/01/2016) 533–539.
[79] J.F. Sarthy, S. Henikoff, K. Ahmad, Chromatin bottlenecks in cancer, Trends Cancer 5 (Mar 2019) 183–194.
[80] R.A. Rupp, P.B. Becker, Gene regulation by histone H1: new links to DNA methylation, Cell 123 (Dec 29 2005) 1178–1179.
[81] S.-M. Yang, B.J. Kim, L. Norwood Toro, A.I. Skoultchi, H1 linker histone promotes epigenetic silencing by regulating both DNA methylation and histone H3 methylation, Proc. Natl. Acad. Sci. Unit. States Am. 110 (2013) 1708.
[82] A. Izquierdo-Bouldstridge, A. Bustillos, C. Bonet-Costa, P. Aribau-Miralbés, D. García-Gomis, M. Dabad, et al., Histone H1 depletion triggers an interferon response in cancer cells via activation of heterochromatic repeats, Nucleic Acids Res. 45 (Nov 16 2017) 11622–11642.
[83] A.S. Grillo, A.M. SantaMaria, M.D. Kafina, A.G. Cioffi, N.C. Huston, M. Han, et al., Restored iron transport by a small molecule promotes absorption and hemoglobinization in animals, Science 356 (May 12 2017) 608–616.
[84] Y.Y. Yien, J. Shi, C. Chen, J.T.M. Cheung, A.S. Grillo, R. Shrestha, et al., FAM210B is an erythropoietin target and regulates erythroid heme synthesis by controlling mitochondrial iron import and ferrochelatase activity, J. Biol. Chem. 293 (Dec 21 2018) 19797–19811.
[85] J. Markert, K. Luger, Nucleosomes meet their remodeler match, Trends Biochem. Sci. 46 (Jan 2021) 41–50.
[86] A.M. Morgan, S.E. LeGresley, K. Briggs, G. Al-Ani, C.J. Fischer, Effects of nucleosome stability on remodeler-catalyzed repositioning, Phys. Rev. E 97 (Mar 2018) 32422.
[87] S. Paul, B. Bartholomew, Regulation of ATP-dependent chromatin remodelers: accelerators/brakes, anchors and sensors, Biochem. Soc. Trans. 46 (Dec 17 2018) 1423–1430.
[88] C.A. Hobbs, B.A. Paul, S.K. Gilmour, Deregulation of polyamine biosynthesis alters intrinsic histone acetyltransferase and deacetylase activities in murine skin and tumors, Cancer Res. 62 (Jan 1 2002) 67–74.
[89] J.A. Biegel, T.M. Busse, B.E. Weissman, SWI/SNF chromatin remodeling complexes and cancer, Am. J. Med. Genet. C Semin. Med. Genet. 166c (Sep 2014) 350–366.
[90] S. Heebøll, M. Borre, P.D. Ottosen, C.L. Andersen, F. Mansilla, L. Dyrskjøt, et al., SMARCC1 expression is upregulated in prostate cancer and positively correlated with tumour recurrence and dedifferentiation, Histol. Histopathol. 23 (Sep 2008) 1069–1076.
[91] H. Takeshima, I. Suetake, S. Tajima, Mouse Dnmt3a preferentially methylates linker DNA and is inhibited by histone H1, J. Mol. Biol. 383 (Nov 21 2008) 810–821.
[92] W.H. Brooks, Increased polyamines alter chromatin and stabilize autoantigens in autoimmune diseases, Front. Immunol. 4 (2013) 91.
[93] S. Sarhan, N. Seiler, On the subcellular localization of the polyamines, Biol. Chem. Hoppe Seyler 370 (Dec 1989) 1279–1284.
[94] K.J. Svensson, J.E. Welch, P. Kucharzewska, P. Bengtson, M. Bjurberg, S. Påhlman, et al., Hypoxia-mediated induction of the polyamine system provides opportunities for tumor growth inhibition by combined targeting of vascular endothelial growth factor and ornithine decarboxylase, Cancer Res. 68 (Nov 15 2008) 9291–9301.
[95] N. Murai, Y. Murakami, A. Tajima, S. Matsufuji, Novel ubiquitin-independent nucleolar c-Myc degradation pathway mediated by antizyme 2, Sci. Rep. 8 (Feb 14 2018) 3005.
[96] H.C. Affronti, M.D. Long, S.R. Rosario, B.M. Gillard, E. Karasik, C.S. Boerlin, et al., Dietary folate levels alter the kinetics and molecular mechanism of prostate cancer recurrence in the CWR22 model, Oncotarget 8 (Nov 28 2017) 103758–103774.
[97] R.G. Schipper, J.C. Romijn, V.M. Cuijpers, A.A. Verhofstad, Polyamines and prostatic cancer, Biochem. Soc. Trans. 31 (Apr 2003) 375–380.
[98] C.E. Massie, I.G. Mills, A.G. Lynch, The importance of DNA methylation in prostate cancer development, J. Steroid Biochem. Mol. Biol. 166 (Feb 2017) 1–15.
[99] K. Fujiwara, G. Bai, T. Kitagawa, D. Tsuru, Immunoelectron microscopic study for polyamines, J. Histochem. Cytochem. 46 (Nov 1998) 1321–1328.
[100] S.M. Whelly, Role of polyamine in the regulation of RNA synthesis in uterine nucleoli, J. Steroid Biochem. Mol. Biol. 39 (Aug 1991) 161–167.
[101] W.H. Brooks, Y. Renaudineau, Epigenetics and autoimmune diseases: the X chromosome-nucleolus nexus, Front. Genet. 6 (22) (2015).
[102] T. Takahashi, Plant polyamines, Plants 9 (Apr 16 2020).
[103] D. Chen, Q. Shao, L. Yin, A. Younis, B. Zheng, Polyamine function in plants: metabolism, regulation on development, and roles in abiotic stress responses, Front. Plant Sci. 9 (2018) 1945.
[104] G.E. Reyna-López, J. Ruiz-Herrera, Specificity of DNA methylation changes during fungal dimorphism and its relationship to polyamines, Curr. Microbiol. 48 (Feb 2004) 118–123.
[105] L. Frostesjö, I. Holm, B. Grahn, A.W. Page, T.H. Bestor, O. Heby, Interference with DNA methyltransferase activity and genome methylation during F9 teratocarcinoma stem cell differentiation induced by polyamine depletion, J. Biol. Chem. 272 (Feb 14 1997) 4359–4366.
[106] A. Pasini, C.M. Caldarera, E. Giordano, Chromatin remodeling by polyamines and polyamine analogs, Amino Acids 46 (Mar 2014) 595–603.

Nucleosome destabilization by polyamines

Laszlo Imre[1]*, Erfaneh Firouzi Niaki[1]*, Rosevalentine Bosire[1], Peter Nanasi Jr.[1], Peter Nagy[1], Zsolt Bacso[1], Nubar Hamidova[1], Yves Pommier[2], Albert Jordan[3], Gabor Szabo[1]**

[1]*Department of Biophysics and Cell Biology, University of Debrecen, Faculty of Medicine Debrecen, H-4032, Hungary*

[2]*Center for Cancer Research, National Cancer Institute, National Institutes of Health, Bethesda, MD 20892-4255, U.S.A.*

[3]*Molecular Biology Institute of Barcelona (IBMB-CSIC), Barcelona, 08028, Spain*

*Contributed equally

**Corresponding author. University of Debrecen, Faculty of Medicine, Department of Biophysics and Cell Biology, Life Science Building, room 2.309. 4032 Debrecen, Nagyerdei krt. 98, Hungary. Email: szabog@med.unideb.hu,

Supplementary material

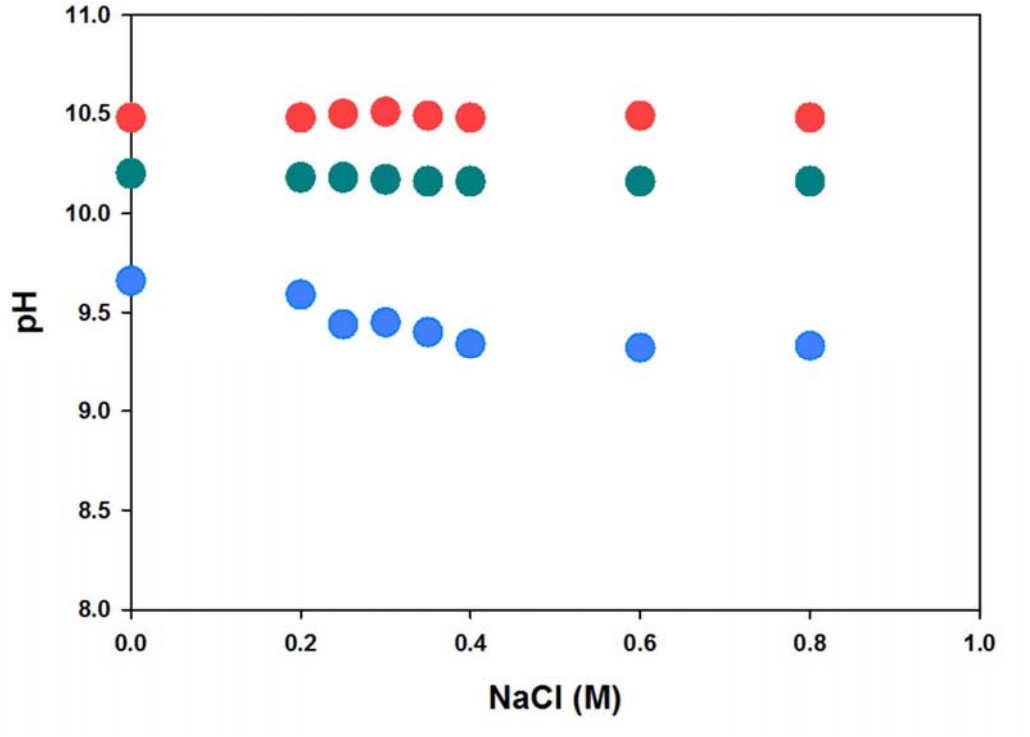

Supplementary Fig. 1. Adjustment of the pH of the solutions used in Figs. 2 and 3.
The pH of the solutions was set to the values shown in the Y axis by the addition of HCl or NaOH. Blue, green and red circles represent solutions containing 2.5, 5 and 10 mM spermidine, respectively. The pH was adjusted by the addition of HCl or NaOH while the change of NaCl cc. was less than ±5 mM.

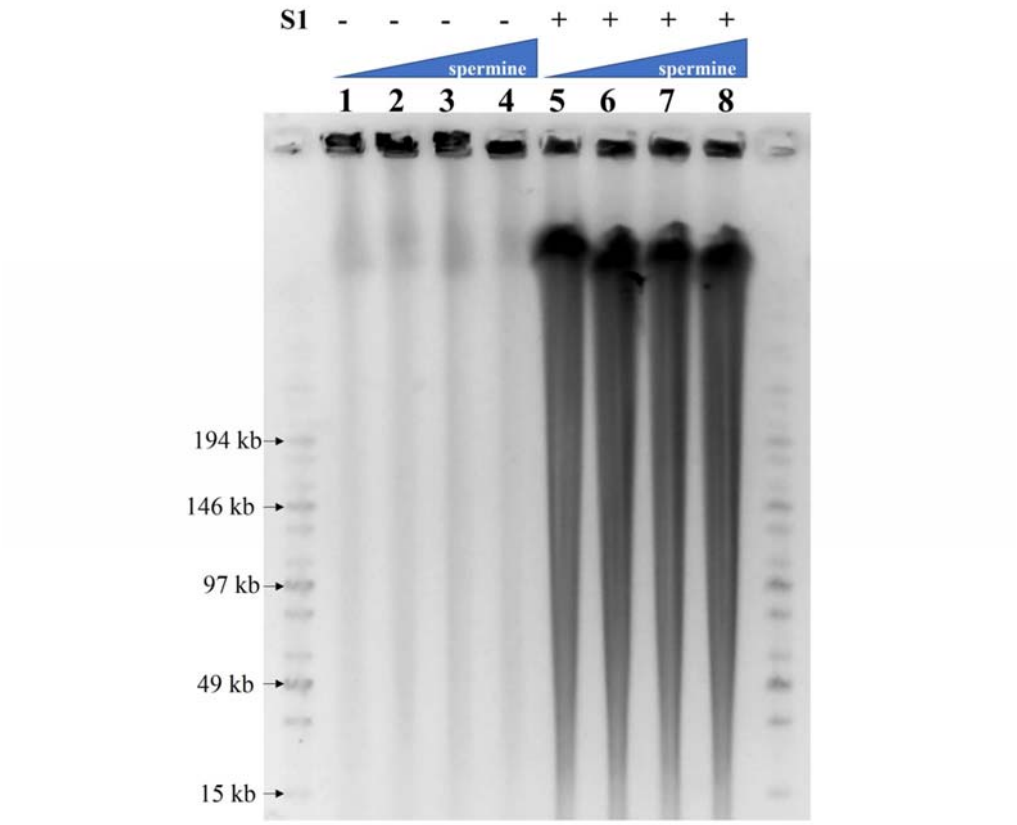

Supplementary Fig. 2.

Pulsed-field gelelectrophoretic analyses of genomic DNA after PA treatment of the permeabilized nuclei.

DNA breaks are not generated as a result of PA treatment. Agarose-embedded HeLa nuclei were treated with spermine applied at 2.5 (lanes 2 and 6), 5 (lanes 3 and 7) and 10 (lanes 4 and 8) mM concentrations, without neutralizing the pH of the PBS/EDTA buffer supplemented with PA. Lanes 1 and 5 show the spermine untreated controls. The deproteinized samples were analyzed by agarose gelelectrophoresis without (samples 1-4), and after treatment with S1 nuclease (samples 5-8). The MidRange PFG marker was used as the DNA ladder. The CHEF protocol used is described in Materials and Methods. The uncropped picture of the gel inverted to grayscale is depicted.

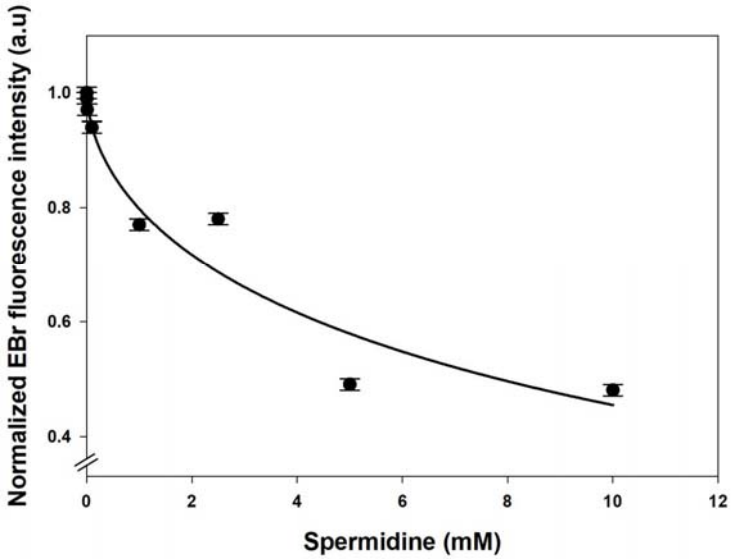

Supplementary Fig 3.

Spermidine binding to DNA demonstrated by EBr displacement in agarose embedded nuclear halos.

Agarose embedded nuclei of Jurkat cells were treated with 2.22 M NaCl/PBS-EDTA to generate nuclei halos which were then stained with 4 µg/ml EBr. Following staining, the dye solutions were replaced with spermidine solutions of the concentration indicated on the X-axis (with their pH set to 7.4); PBS-EDTA was used in the case of the control. The red fluorescence of EBr was quantified by LSC and the data analyzed by the iCys software. The graph was prepared by SigmaPlot and data fitted by the four-parameter logistic curve. The graph shows the mean ± SEM of EBr fluorescence intensities of 200-1,000 G0/G1 nuclei normalized to the control (without spermidine treatment).

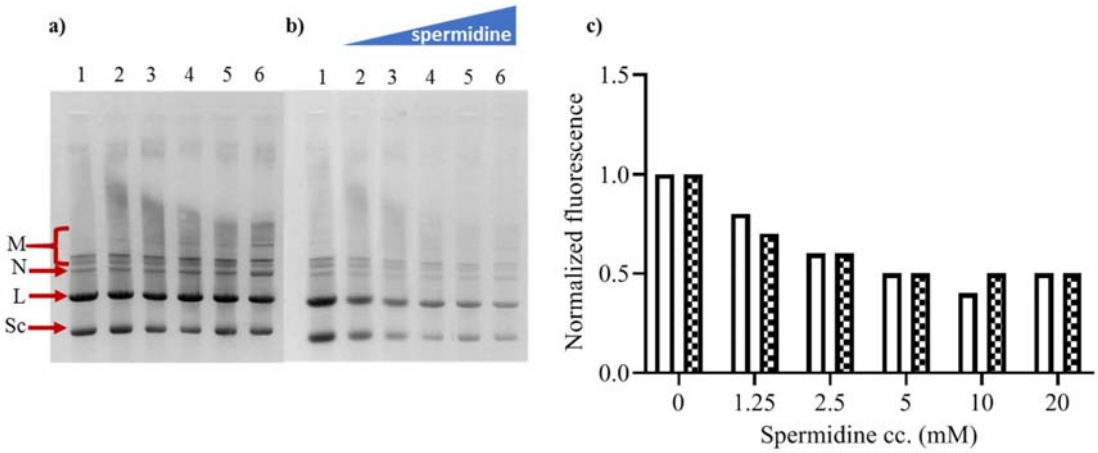

Supplementary Fig 4. Comparison of PA binding of different topological forms of plasmid DNA.

Spermidine displaces EBr equally from the different topological forms of DNA. DNA samples containing linear, nicked and supercoiled plasmid DNA in equal proportion (0.5µg each) were electrophoresed on a 1% agarose gel and then stained with 0.5 µg/ml EBr. After imaging, individual lanes were cut out and incubated with varying concentrations of spermidine, followed by a second imaging. The reduction in band intensity was quantified using Fiji ImageJ. **a)** EBr stained gel image of identical plasmid DNA samples before spermidine treatment showing the separated supercoiled (Sc), linear (L), nicked (N) forms and multimers (M). **b)** Gel image of EBr stained plasmid DNA subjected to 0, 1.25, 2.5, 5, 10 and 20 mM spermidine; lanes 1-6, respectively. In **a)** and **b)** the uncropped pictures of the gel inverted to grayscale are depicted. In panel **c)** the fractions of EBr bound to the supercoiled (empty bars) and linear (checkered bars) topological forms after subjecting the EBr stained bands to the indicated amounts of spermidine are shown.

A

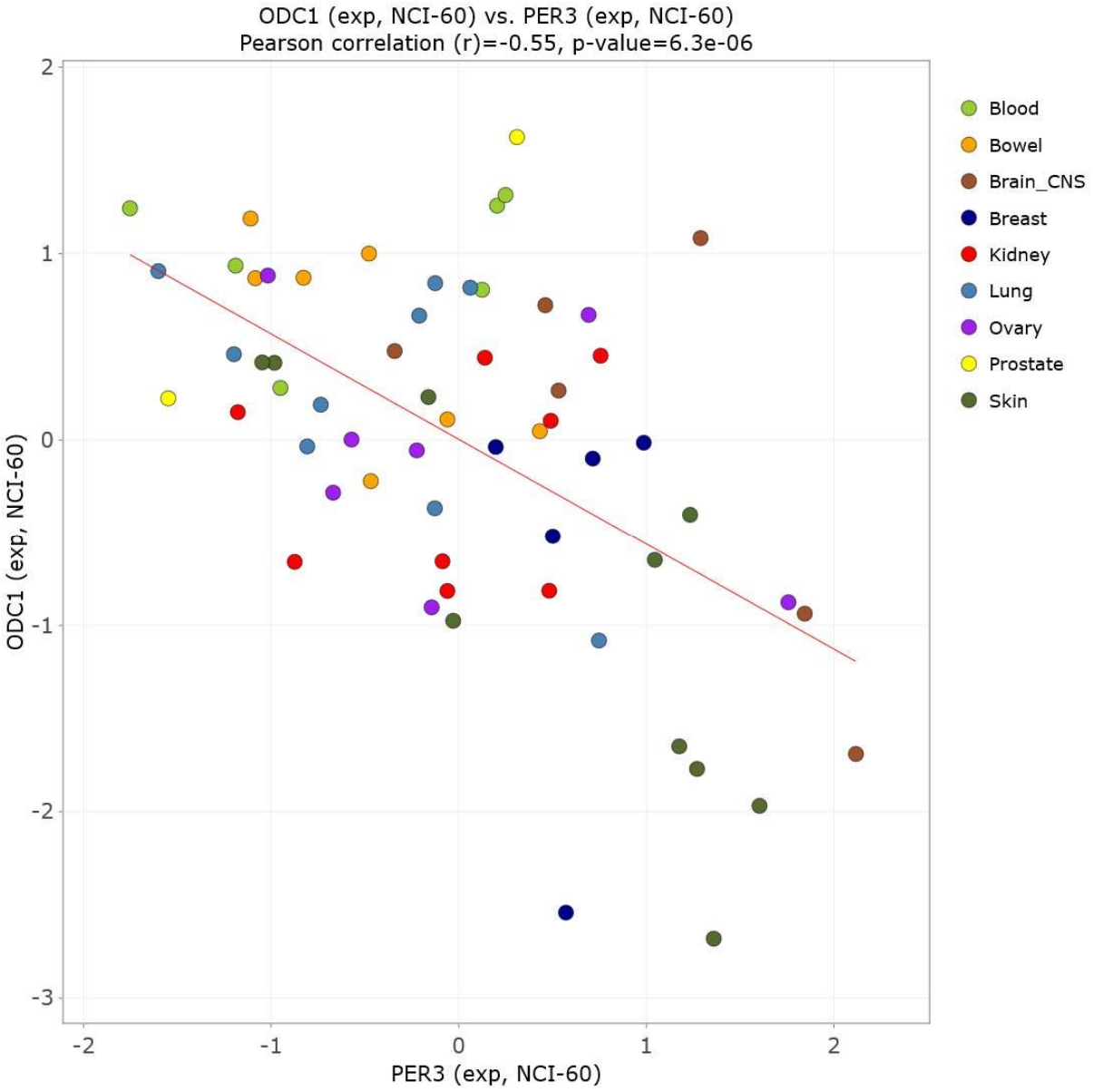
ODC1 (exp, NCI-60) vs. PER3 (exp, NCI-60)
Pearson correlation (r)=-0.55, p-value=6.3e-06
ODC1 (exp, NCI-60)
PER3 (exp, NCI-60)
2
1
0
-1
-2
-3
-2
-1
0
1
2
Blood
Bowel
Brain_CNS
Breast
Kidney
Lung
Ovary
Prostate
Skin

B

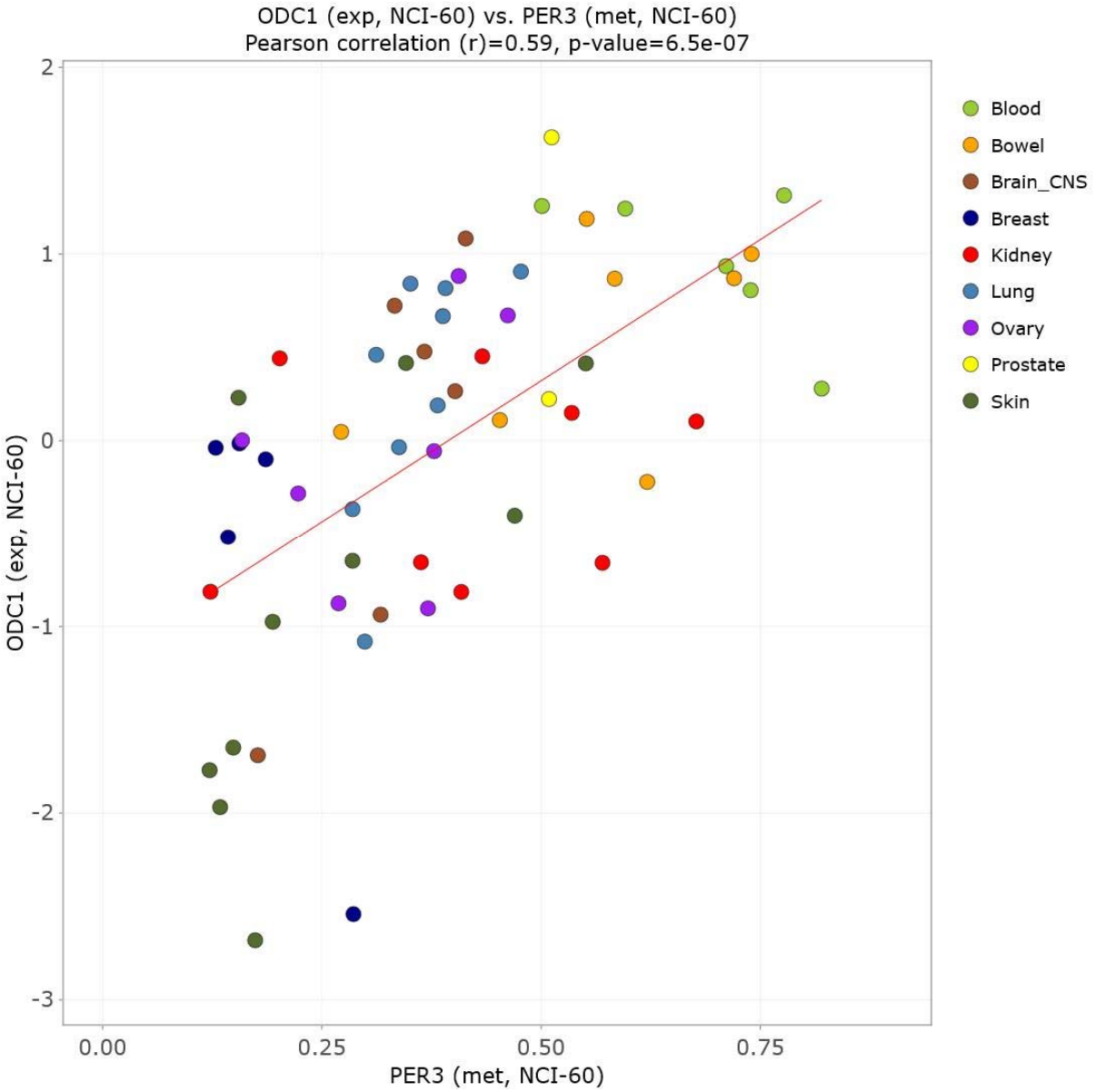

Supplementary Figure 5. CellMiner analyses based on the NCI60 cell line panel, using CellMinerCDB.

A. Correlation between ODC1 and PER3 mRNA expression.

B. Correlation between ODC1 mRNA expression and PER3 DNA methylation.

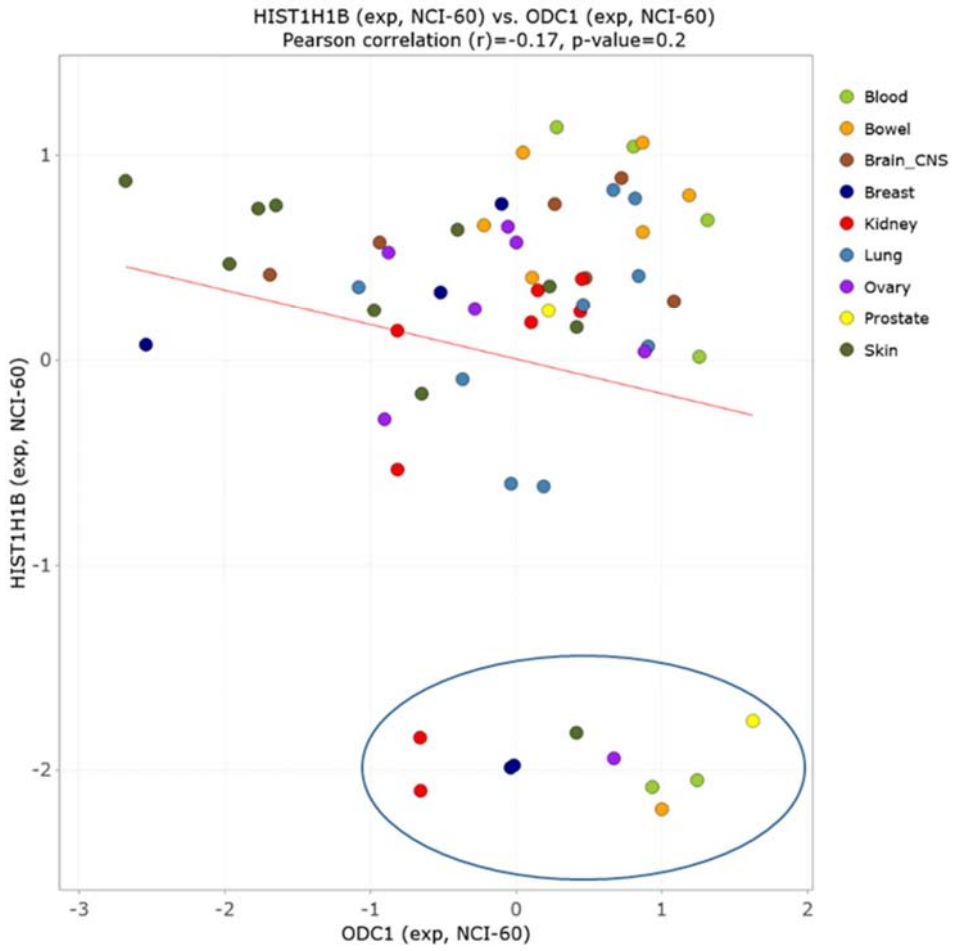

Supplementary Fig 6.

CellMiner analyses based on the NCI60 cell line panel, using CellMinerCDB.

A distinct subpopulation of ten cell lines of varied lineages (encircled) exhibits a very low expression of the gene coding for the histone variant H1.5, and high ODC1 expression on average at the same time. The ten cell lines: HCT-116; A498; HL-60; RPMI-8226; MDA-MB-231; HS578T; OVCAR-3; ACHN; LOXIMVI; PC-3.

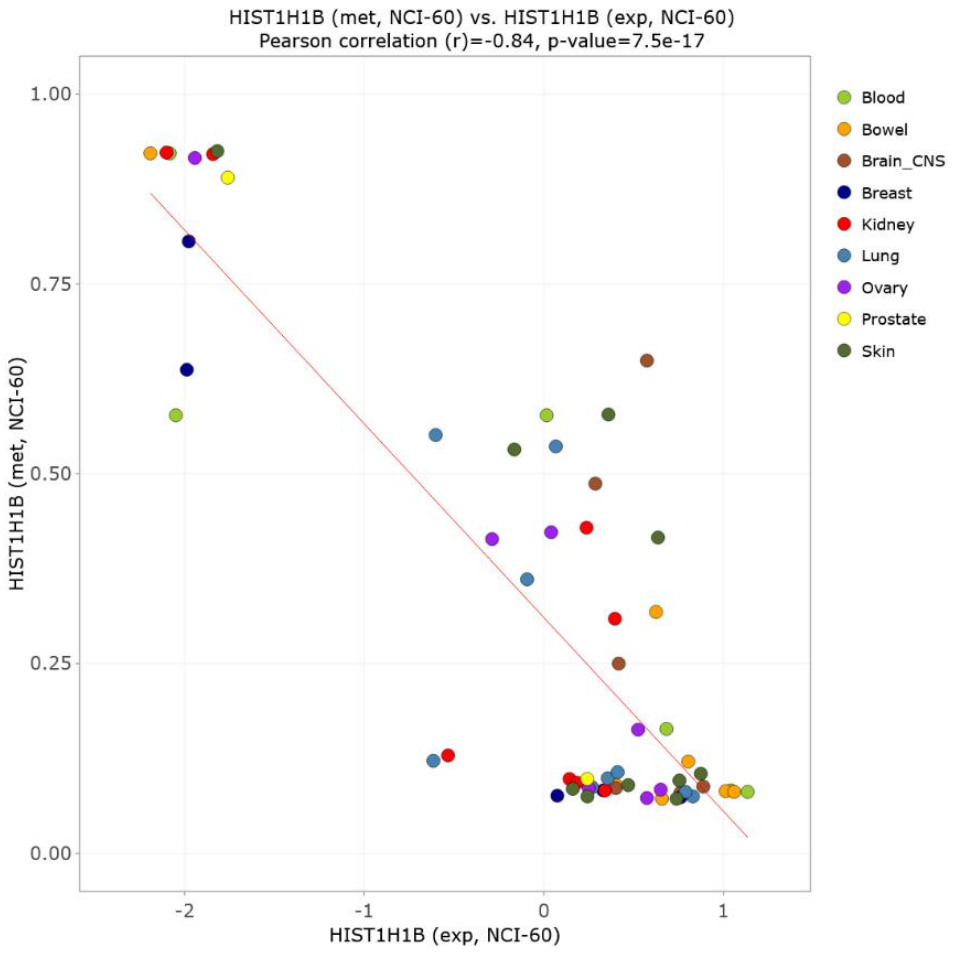

Supplementary Figure 7.

CellMiner analyses based on the NCI60 panel, using CellMinerCDB.

Low HIST1H1B expression correlates with high CpG methylation of the same genomic region in the same subpopulation of cell lines.

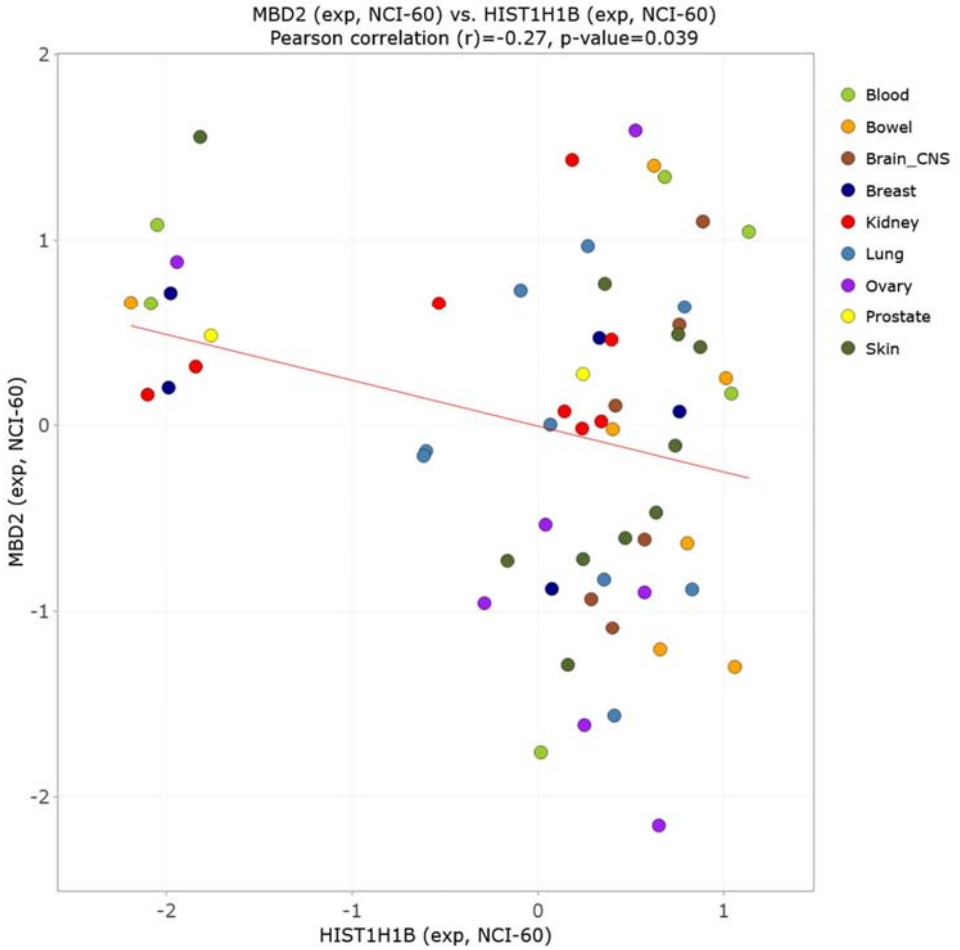

Suppl. Figure 8. CellMiner analyses based on the NCI60 panel, using CellMinerCDB.

Low HIST1H1B correlates with high MBD2 expression in the same ten cell lines.

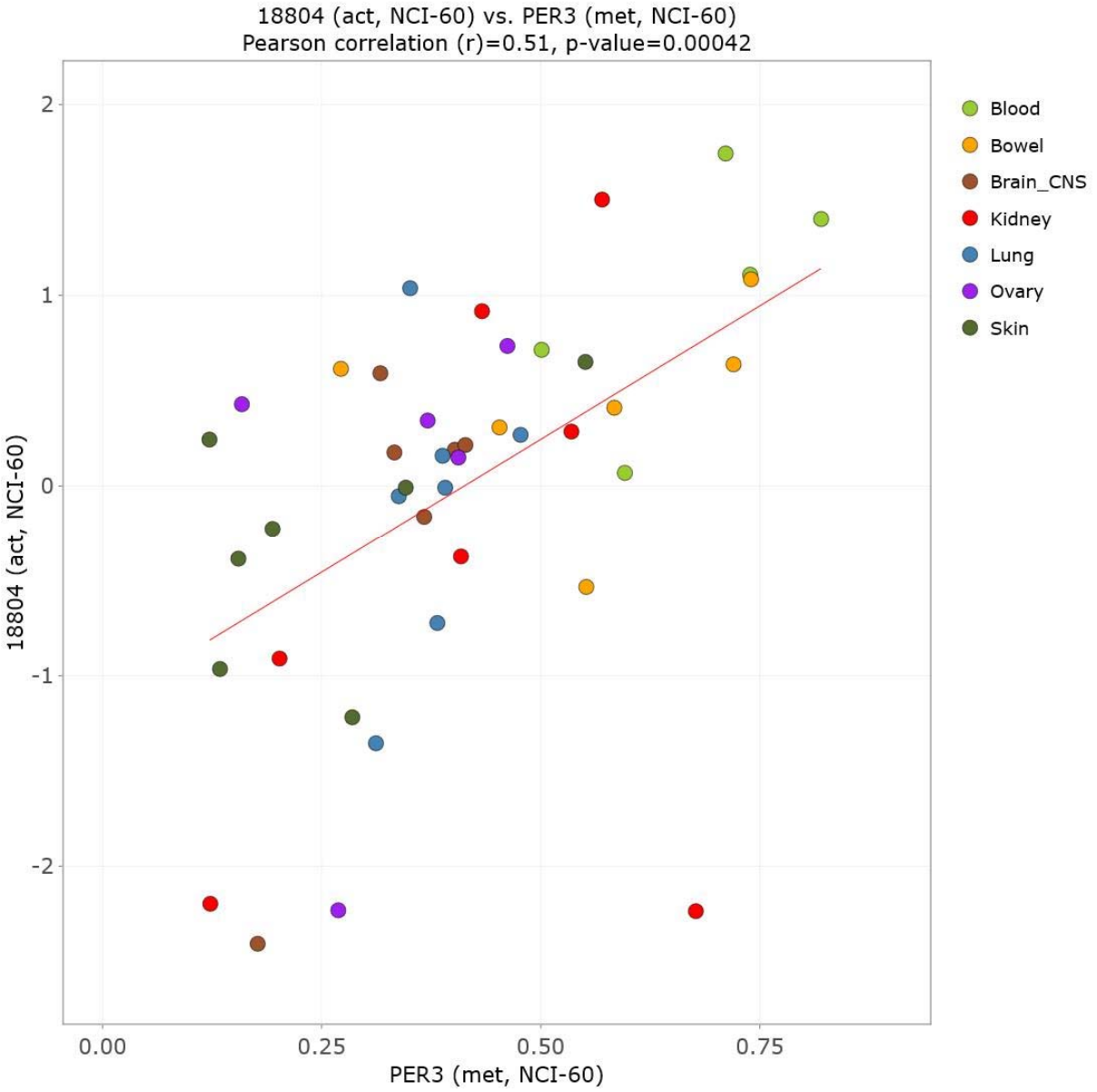

Supplementary Figure 9. CellMiner analyses based on the NCI60 panel, using CellMinerCDB.

Silencing of PER3 via DNA methylation correlates with Hinokitiol toxicity across the NCI60 cell line panel.